Asociación Argentina
de Mecánica Computacional

Mecánica Computacional Vol XXV, pp. 2573-2583
Alberto Cardona, Norberto Nigro, Victorio Sonzogni, Mario Storti. (Eds.)
Santa Fe, Argentina, Noviembre 2006

NUMERICAL SIMULATION OF ELECTROKINETIC FLOW IN MICROFLUIDIC CHIPS

Fabio A. Guarnieri[a,b], Pablo A. Kler[a] and Claudio L. A. Berli[c,d]

[a]CIMEC, INTEC (UNL-CONICET), PTLC, El Pozo, 3000, Santa Fe, Argentina.
[b]Fac. de Bioingeniería, UNER, 3100, Oro Verde, Argentina.
[c]INTEC (UNL-CONICET), Güemes 3450, 3000, Santa Fe, Argentina.
[d]Dpto. de Física, Fac. de Bioquímica y Cs. Biol., UNL, El Pozo, 3000, Santa Fe, Argentina.

Keywords: Microfluidics, microchannel networks, electrokinetic flow, analytical devices.

Abstract. Microfluidic chips are miniaturized analytical devices used in chemical, biological and medical applications. In most cases, fluids are conducted through microchannels by applying electric potentials and/or pressure gradients. This growing lab-on-a-chip technology requires numerical simulations to assist the design, control and optimization of analytical manipulations. The present work deals with FEM-based calculations of the dynamics of electrolyte solutions in cross-shaped microchannels, where the flow is driven by the action of external electric fields. A theoretical modeling of electrokinetic and transport phenomena in the system is carried out in the framework of continuum fluid mechanics. Calculations ground on conservation equations of mass, momentum and electrical charge, considering effects in three dimensions. Operations normally performed in analytical systems are discussed, such as loading, focusing, and injection of samples. Numerical simulations carried out in this work can be a valuable tool to control and optimize practical manipulations in microfluidic chips.

1 INTRODUCTION

Microfluidic chips or microscale total analysis systems (μTAS) perform the functions of large analytical devices in small, often disposable, units (Reyes , 2002). The benefits of μTAS are a reduction of consumption of samples and reagents, shorter analysis times, greater sensitivity, portability and disposability. There has been a huge interest in these devices in the past decade that led to a commercial range of products by Caliper, Agilent, Shimadzu and Hitachi (Freemantle, 1999).

Most microfluidic systems have been successfully fabricated in glass or oxidized silicon (Si/SiO2) (Madou, 2002). Microscopic channels are defined in these substrates using photolithography and micromachining, whose materials and fabrication methods were adopted from the developed microelectronics industry. But for rapid prototyping and testing of new concepts, which is the aim of our group, the fabrication processes are slow and expensive. Computational and analytical simulation of on-chip processes, can serve to reduce the time from concept to chip (Erickson, 2005). However, there are complications like the several orders of magnitude of the relevant length scales involved like the electric double layer (EDL) thickness (in nm) and microchannels length (in mm). This EDL is an interfacial phenomenon whose importance is increased because of the scale downsizing. But, in general and the most challenging and interesting aspect of computational simulation of microfluidic chips is the multiphysics nature which combines fluidics, transport, thermal, mechanics, electronics and optics with chemical, biological thermodynamics and reaction kinetics.

Some of the first numerical simulations of flow and species transport for microfluidic chips were based on electrokinetic focusing and sample dispensing techniques. Patankar and Hu (1998) and Ermakov et al. (1998, 2000) employed an algorithm based on a finite volume discretization of the governing equations on a grid to simulate those techniques. Bianchi et al. (2000) performed 2D finite element simulations artificially increasing the EDL thickness. 3D finite volume simulations have been also performed (Sundararajan et al., 2004, MacInnes et al., 2003). Erickson and Li (2004) investigated electro-osmotic flow (EOF) in heterogeneous surfaces with a 3D finite element model on a simultaneous solution to the Nernst-Planck, Poisson and Navier-Stokes equations.

In this paper, a 3D finite element model is developed for the simulation of an electro-osmotic flow in rectangular microscale channel networks. Calculations are carried out in 3 steps: first, solving the potential distribution arising from the external electric field; second, these distributions are inserted in the Navier-Stokes equation for the calculation of the velocity profile; finally, for the sample transport, a solution of the convection-diffusion equation for one species is found. The EDL effect is introduced by means of a slip velocity, provided the EDL thickness is small in comparison with the channel depth. This approximation reduces the complexity of the mesh and the computational cost.

The paper is organized as follows. Fundamental aspects of transport phenomena in microfluidic networks are summarized in Section 2. Then the particular problem of cross-shaped microchannels is formulated in Section 3, where the final set of equations is outlined. The numerical scheme used is described in Section 4, and finally, different examples of application are discussed in Section 5.

2 THEORETICAL FRAMEWORK

2.1 Governing Equations

Electrokinetic and transport phenomena in micro-scale devices can be treated in the

framework of continuum fluid mechanics (Stone et al., 2004). Therefore, we start from the following set of coupled equations that relate fluid velocity (u), pressure (p) and electric field (E) in the flow domain of microchannels (Probstein, 1989; Hunter, 1992; Li, 2004),

$$\frac{\partial \rho}{\partial t} + \underline{\nabla} \cdot (\rho \underline{u}) \tag{1}$$

$$\rho\left(\frac{\partial \underline{u}}{\partial t} + \underline{u} \cdot \underline{\nabla}\underline{u}\right) = -\underline{\nabla} p + \mu \nabla^2 \underline{u} + \rho \underline{g} + \rho_e \underline{E} \tag{2}$$

$$\varepsilon \underline{\nabla} \cdot \underline{E} = \rho_e \tag{3}$$

$$\frac{\partial c_s}{\partial t} + \underline{u} \cdot \underline{\nabla} c_s = D_s \nabla^2 c_s \tag{4}$$

Equation 1 expresses the conservation of mass for incompressible fluids. Equation 2 (Navier-Stokes equation) expresses the conservation of momentum for Newtonian fluids of viscosity μ and density ρ, subjected to gravitational field of acceleration g and electric field intensity E. The last term on the RHS of equation 2 represents the contribution of electrical forces to the momentum balance, where $\rho_e = e\sum_k z_k c_k$ is the electric charge density of the electrolyte solution, obtained as the summation over all type-k ions, with valence z_k and number density c_k (mol/m^3); e is the elementary charge.

Equation 3 (Poisson equation) establishes the relation between electric potential and charge distributions in the fluid of permittivity ε. Here it is relevant to mention that the ion distributions c_k (to be included in equations 2 and 4 through ρ_e) must be derived from Nerst-Plank equation, which accounts for the flux of type-k ions due to electrical forces, fluid convection and Brownian diffusion (Probstein, 1989). In the present work we avoid this coupling by introducing a suitable simplification (see below, Section 2.2).

Equation 4 (convective-diffusion equation) describes the transport of a sample (s) consisting of electrically neutral molecules with diffusion coefficient D_s. It is worth noting that when molecules to be transported are electrically charged, electrophoretic transport must be taken into account by including an additional term in equation 4 (electric forces on particles). This possibility is of interest in separation processes, and it is out of the scope of the present work, which is addressed to basic manipulations in microfluidic chips.

Finally, it should be mentioned that an important effect associated with electric current in microchannels is temperature rising due to internal heat generation, namely Joule effect (for example, Li, 2004). In this sense, the present modeling assumes that temperature is constant and uniform throughout the system. Otherwise, a thermal balance equation must be coupled to equations 1-4, which, in turn, must include the temperature dependence of coefficients ρ, μ, ε and D_s.

2.2 Fundamentals of EOF and 'Slip Velocity' Approximation

EOF grounds on the existence of electrostatic charges in the interface between the channel walls and the fluid. In principle, it may be thought that solid walls expose toward the fluid a certain number of specific sites able to release or take H^+ ions. In equilibrium with an aqueous electrolyte solution, the surface becomes electrically charged (typically, negative) with a surface potential on the order of 50 mV. This potential decreases, and then vanishes in the

liquid phase, because of the screening produced by counterions and other electrolyte ions in solution, which constitute the EDL. The thickness of this layer is quantified through Debye length (Probstein, 1989; Hunter, 1992),

$$\lambda = \left(\frac{\varepsilon RT}{e^2 \sum_k z_k^2 c_k^b} \right)^{1/2} \tag{5}$$

where c_k^b is the bulk concentration of the k-th ion, R is the gas constant and T is the absolute temperature. For the ionic concentrations normally used in practice, λ is on the order of 10 nm. Away from the interface, at distances beyond λ, the bulk of the fluid is electrically neutral.

When an external electric field is applied tangent to the interface, in the axial direction of the channel, the electric forces acting on excess ions in the EDL drag the surrounding liquid, and thus EOF develops. For thin EDL in relation to the channel width (h), the effect is confined to a certain plane parallel to the channel wall, also designated shear plane, where the surface potential is the so-called electrokinetic ζ-potential. Under these conditions, the electro-osmotically driven flow can be regarded as the result of an electrically-induced 'slip velocity', the magnitude of which is (Probstein, 1989; Hunter, 1992),

$$\underline{u}_{EO} = \frac{\varepsilon \zeta}{\mu} \underline{E} \tag{6}$$

Further, $\underline{u}_{EO}$ can be used as a boundary value at the channel walls. This possibility greatly simplifies calculations since ion distributions c_k are de-coupled from Navier-Stokes and Poisson equations. In fact, if ion concentrations are assumed to be uniform (except in the close vicinity of the charged interface), and hence $\rho_e \approx 0$ throughout the flow domain, the RHS of equation 3 vanishes, as well as the last term of equation 2. The approximation is valid for large values of h/λ, which is usually the case in micro-scale channels at moderate ionic concentrations (~10^{-3} M). Nevertheless, at very low ionic concentrations (~10^{-6} M), or in case of nano-scale channels, h/λ approaches 1, indicating that the EDL from opposing surfaces overlap. In that case, equation 6 does not apply and the full problem must be solved.

3 3D-MODEL OF CROSS-SHAPED MICROCHANNELS

3.1 Definition of the Problem

In this work we consider straight microchannels of length l with a cross-shaped intersection, as shown schematically in Fig. 1a. A Cartesian coordinate system is used, with channels placed in the x-y plane, and the origin (0, 0, 0) at the intersection. The rectangular cross-section of microchannels is presented in Fig. 1b, where depth h and width w are defined. In addition, the x-y plane containing the microchannels is considered to be perfectly horizontal, so that no pressure gradients due to gravity take place.

The external electric field along the channels is established by applying well-defined electrical potentials ϕ_i in each one of channel ends (i = 1 to 4, reservoirs in practice). Therefore, $\underline{E} = -\underline{\nabla}\phi$ is applied in x and y directions only. Under the circumstances, and considering microchannels of equal topography and surface properties, the relative values of electric field intensity in each branch can be predicted beforehand by using Kirchoff laws of

electrical circuits, that is, $\sum_i E_{x,i} = \sum_i E_{y,i}$ (Ermakov et al., 2000; Lin et al., 2002).

In relation with start-up flow, different authors (Patankar and Hu, 1998; MacInnes, 2002; Stone et al., 2004) consider that the time required to reach the steady state can be roughly measured as $t_{ss} \approx \rho h^2/\mu$, which is in the order of 10^{-4} s for aqueous solutions in micro-scale channels. Therefore, the electrokinetic flow in typical operations like sample loading and injection is practically a steady state flow. For the sake of simplicity, in what follows we drop out the temporal derivative of Navier-Stokes equation.

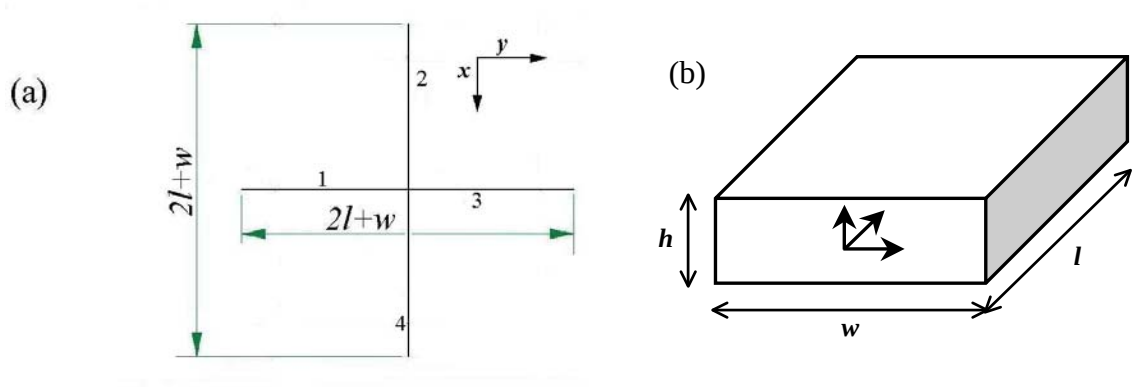

Figure 1: Schematical representations of (a) cross-shaped microchannel network, and (b) 3D design of rectangular microchannels. Geometrical definitions and coordinate system used in calculations are also included.

3.2 Equations for numerical computations

According to the definitions and approximations described above, equations 1-4 are re-written as follows,

$$\frac{\partial u_x}{\partial x} + \frac{\partial u_y}{\partial y} + \frac{\partial u_z}{\partial z} = 0 \tag{7}$$

$$\rho\left(u_x\frac{\partial u_x}{\partial x} + u_y\frac{\partial u_x}{\partial y} + u_z\frac{\partial u_x}{\partial z}\right) = -\frac{\partial p}{\partial x} + \mu\left(\frac{\partial^2 u_x}{\partial x^2} + \frac{\partial^2 u_x}{\partial y^2} + \frac{\partial^2 u_x}{\partial z^2}\right) \tag{8a}$$

$$\rho\left(u_x\frac{\partial u_y}{\partial x} + u_y\frac{\partial u_y}{\partial y} + u_z\frac{\partial u_y}{\partial z}\right) = -\frac{\partial p}{\partial y} + \mu\left(\frac{\partial^2 u_y}{\partial x^2} + \frac{\partial^2 u_y}{\partial y^2} + \frac{\partial^2 u_y}{\partial z^2}\right) \tag{8b}$$

$$\rho\left(u_x\frac{\partial u_z}{\partial x} + u_y\frac{\partial u_z}{\partial y} + u_z\frac{\partial u_z}{\partial z}\right) = -\frac{\partial p}{\partial y} + \mu\left(\frac{\partial^2 u_z}{\partial x^2} + \frac{\partial^2 u_z}{\partial y^2} + \frac{\partial^2 u_z}{\partial z^2}\right) \tag{8c}$$

$$\frac{\partial^2 \phi}{\partial x^2} + \frac{\partial^2 \phi}{\partial y^2} + \frac{\partial^2 \phi}{\partial z^2} = 0 \tag{9}$$

$$\frac{\partial c_s}{\partial t} + u_x\frac{\partial c_s}{\partial x} + u_y\frac{\partial c_s}{\partial y} + u_z\frac{\partial c_s}{\partial z} = D_s\left(\frac{\partial^2 c_s}{\partial x^2} + \frac{\partial^2 c_s}{\partial y^2} + \frac{\partial^2 c_s}{\partial z^2}\right) \tag{10}$$

This set of equations defines the three-dimensional flow in cross-shaped microchannels, and thus constitute the problem to be solved numerically. It is worth to remember that the electrokinetic effect is associated to the 'slip velocity' at the walls, as expressed below.

3.3 Boundary Conditions

Following the discussion given in Section 23.2, the boundary values to be imposed at the **channel walls** are:
a) Branches in *x*-direction,

$$y = \pm w/2\ ,\ u_x = \frac{\varepsilon\zeta}{\mu}\frac{\partial\phi}{\partial x}\ ,\ u_y = 0\ ,\ \frac{\partial\phi}{\partial y} = 0\ ,\ \frac{\partial c_s}{\partial y} = 0\ ; \tag{11}$$

$$z = \pm h/2\ ,\ u_x = \frac{\varepsilon\zeta}{\mu}\frac{\partial\phi}{\partial x}\ ,\ u_z = 0\ ,\ \frac{\partial\phi}{\partial z} = 0\ ,\ \frac{\partial c_s}{\partial z} = 0\ ; \tag{12}$$

b) Branches in *y*-direction,

$$x = \pm w/2\ ,\ u_y = \frac{\varepsilon\zeta}{\mu}\frac{\partial\phi}{\partial y}\ ,\ u_x = 0\ ,\ \frac{\partial\phi}{\partial x} = 0\ ,\ \frac{\partial c_s}{\partial x} = 0\ ; \tag{13}$$

$$z = \pm h/2\ ,\ u_y = \frac{\varepsilon\zeta}{\mu}\frac{\partial\phi}{\partial y}\ ,\ u_z = 0\ ,\ \frac{\partial\phi}{\partial z} = 0\ ,\ \frac{\partial c_s}{\partial z} = 0 \tag{14}$$

where the zero-potential gradient normal to interfaces express the insulation condition.

In addition, fully developed flows are assumed in both **entry** and **exit regions** of the channels. Thus the conditions to be imposed at channels ends are:
a) Branches in *x*-direction,

$$x = \pm(l + w/2)\ ,\ u_y = u_z = 0\ ,\ \frac{\partial u_x}{\partial x} = 0\ ,\ p = p_i\ ,\ \phi = \phi_i\ . \tag{15}$$

b) Branches in *y*-direction,

$$y = \pm(l + w/2)\ ,\ u_x = u_z = 0\ ,\ \frac{\partial u_y}{\partial y} = 0\ ,\ p = p_i\ ,\ \phi = \phi_i\ . \tag{16}$$

Furthermore, when a **sample** is transported by the flow, the following conditions are used:

$$t \le 0\ ,\ c_s = 0\ \text{(throughout the flow domain)} \tag{17}$$

$$t > 0\ ,\ y = -(l + w/2)\ ,\ c_s = c_0\ \text{(inlet of channel 1)} \tag{18a}$$

$$y = (l + w/2)\ ,\ \frac{\partial c_s}{\partial y} = 0 \tag{18b}$$

$$x = \pm(l + w/2)\ ,\ \frac{\partial c_s}{\partial x} = 0 \tag{18c}$$

Therefore, by solving equations 7-10 with boundary conditions 11-18, one simultaneously obtains the velocity, pressure, electric potential and concentration fields developed in the

cross-shaped microchannel. Next step consist in defining the numerical scheme for calculations.

4 NUMERICAL SCHEME

For the discretization of the Navier-Stokes equation for incompressible flow (equations 7, 8a-c) we choose some basis spaces V^h, Q^h for the approximation of u and p, and apply the Galerkin method. Quadratic and linear interpolation are chosen for u and p, respectively, (Q2P1) to satisfy the Babuška-Brezzi inf-sup condition. For the discretization of the Poisson equation (equation 9) and the diffusion-convection equation (equation 10), Galerkin method is used with quadratic interpolation. An implicit method is used for the discretization of the time domain. Newton-Raphson method is used to solve the nonlinear problem with a direct solver. The simulations are carried out in a dual core AMD Opteron, processor 265, 1.81 Ghz, 7.25 Gb RAM under Windows XP 64 bits.

5 EXAMPLES OF ILLUSTRATION

In this section we discuss some simple manipulations performed in analytical microsystems, in order to illustrate the applications of the 3D numerical model. First we describe briefly how these operations are carried out in practice (see for example, Li, 2004 for further details). Microchannels are filled with an electrolyte solution of defined ionic concentration. Then, in the **loading** step, a sample added to the inlet of channel 1 is transported by the fluid towards channel 3, which is achieved by applying an appropriate combination of electric potentials to channel ends. Once the sample plug reached the intersection, potentials are conveniently switched, so that flow is established in channels 2 and 4, and simultaneously stopped in channels 1 and 3. Thus, in the so-called **injection** step, a fraction of the sample plug is taken from the intersection and conducted through the transverse channel. In addition, to handle the size of the sample before the injection, the operation known as **focusing** is carried out. This basically consists in controlling the relative flow rate of channels 1, 2 and 4 during the loading step, by modifying the applied electric potentials.

In the examples below, the geometrical dimensions of microchannels are l = 25 mm, w = 0.1 mm, and h = 40 μm. The electrokinetic potential is defined to be ζ = –40 mV. Circulating fluids are aqueous electrolyte solutions at 20°C, thus ρ = 1000 kg/m^3, $\mu = 10^{-3}$ Ns/m^2, and ε = 7.1 10^{-10} C^2/Jm. The ionic concentration used in all cases is 10^{-3} M, which yields $\lambda \approx 10$ nm. Therefore, since $h/\lambda \approx 4000$, the 'slip velocity' approximation (Section 2.2) applies in our calculations here. The diffusion coefficient of the sample is $D_s = 2\ 10^{-9}$ m^2/s.

5.1 Loading

In the loading process, the challenge is achieving a precise control of the sample velocity, and avoiding sample leakage to transverse channels. The correct performance for the system is obtained by controlling the applied potentials at the ends of the channels. In this sense, the symmetry in geometrical and surface properties of channels provides several practical advantages. The most important one is the possibility of using a single voltage source for the system. In fact, according to Kirchoff´s law (see above Section 3.1), the potential value at the center of the intersection is $\phi_c = \frac{1}{4}(\phi_1 + \phi_2 + \phi_3 + \phi_4)$, where ϕ_1, ϕ_2, ϕ_3 and ϕ_4 are the potentials applied to channel ends. Therefore, taking advantage of the symmetry of the microfluidic circuit considered, operations like sample loading, focusing and injection can be done by

using a fixed value voltage source.

In this particular example we consider the transport of fluid from channel 1 to 3, avoiding flow through channels 2 and 4. This is done by applying a potential distribution as follows: $+\phi_0$ to channel 1, GND to channels 2 and 4, and $-\phi_0$ to channel 3, with ϕ_0 ranging from 50 to 600 V. Typical results of fluid velocity and electrical potential distributions obtained under these conditions are presented in Figs. 2a and b, respectively. Furthermore, numerical values of the flow rate in each branch were obtained by integrating the velocity profile in the cross-sectional area, at distances far enough from both channel ends and central intersection. On the other hand, the respective flow rates predicted by unidirectional models of electro-osmotic flow (Probstein, 1989; Li, 2004) were calculated for the same electric potentials. The relative difference between flow rate values was found to be on the order of 10^{-3}. This comparison is possible because microchannels considered are sufficiently thin (l/w = 250), and it serve us to validate 3D calculations.

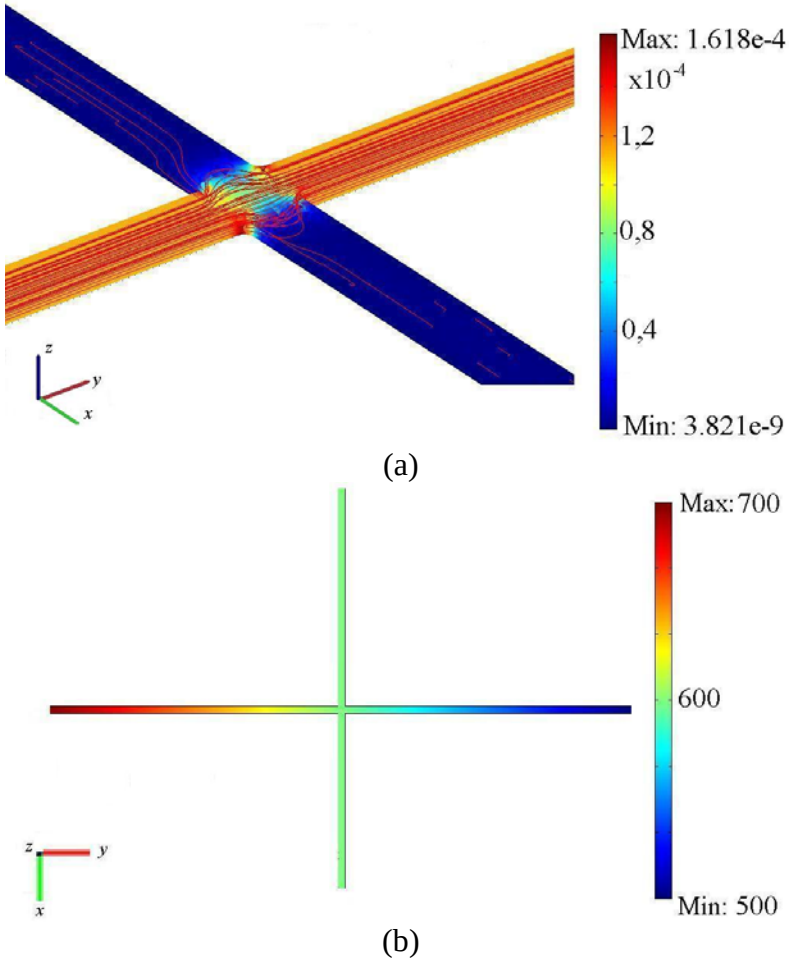

Figure 2: (a) Fluid velocity (m/s) and (b) electric potential (V) fields developed in the vicinity of channel intersection during a typical operation of sample loading. Numerical values for calculations are given in the text.

5.2 Focusing

Sample injection in a microfluidic chip is one of the key steps in (chemo-) analytical operations, and its characteristics determine the quality of both separation and detection

processes. As mentioned above, in some cases it may be necessary to provide a sample plug of smaller volume for the separation process. For this purpose, the volume of the sample plug in the loading step may be controlled by confining the sample stream (from channel 1 towards channel 3) between the fluid streams from channels 2 and 4. This procedure is able to generate well defined extent sample plugs, suitable for high performance separations.

The example shown in Figure 3 involves a voltage distribution compatible with the aforementioned simple source criteria. In fact, here we adopt $\phi_1 = \phi_2 = \phi_4 = 1200$ V, and $\phi_3 =$ GND, to obtain the minimum volume plug attainable with the fixed potential source system. For this example we assume that the sample has a fixed concentration $c_0 = 25$ mol/m^3 at the inlet of channel 1. The figure shows the concentration distribution for a time long enough to consider $\partial c_s/\partial t \approx 0$ in equation 10.

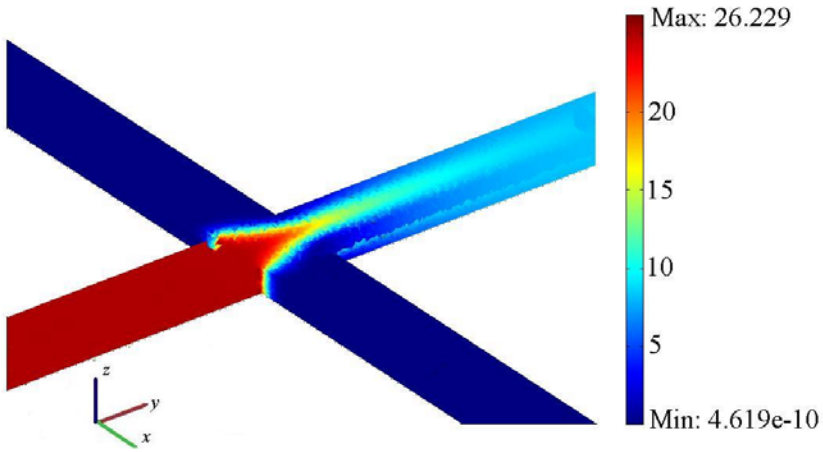

Figure 3:Simulation of sample concentration distribution (mol/m^3) typically obtained by focusing operation. Numerical values for calculations are given in the text.

5.3 Injection

During this operation, the sample must be confined in a small moving region in which the concentration is as uniform as possible, in order to improve subsequent separation and detection processes. Figures 4a-d present some results of numerical simulations carried out in this work. After loading and focusing, once the sample has conveniently reached the intersection (Fig. 4a), the potential distribution is switched to inject a fraction of the sample volume to channel 4. At this step, we implemented the following potential distribution: $\phi_1 = \phi_3 =$ GND, $\phi_2 = +\phi_0$, $\phi_4 = -\phi_0$, where $\phi_0 = 600$V (it is worth noting that this potential distribution is also attained with a single source). Figures 4b to 4d show the temporal evolution of the sample concentration field. The time considered for the simulation ranged between 0 (initial step, Fig. 4a) and 0.6 s (Fig. 4d). Also in this case, $c_0 = 25$ mol/m^3 at the inlet of channel 1, while initial boundary conditions are those outlined in Section 3.3. In particular, when potentials are switched, the background sample concentration (Fig. 4a) is that calculated in the previous example (focusing, Figure 3).

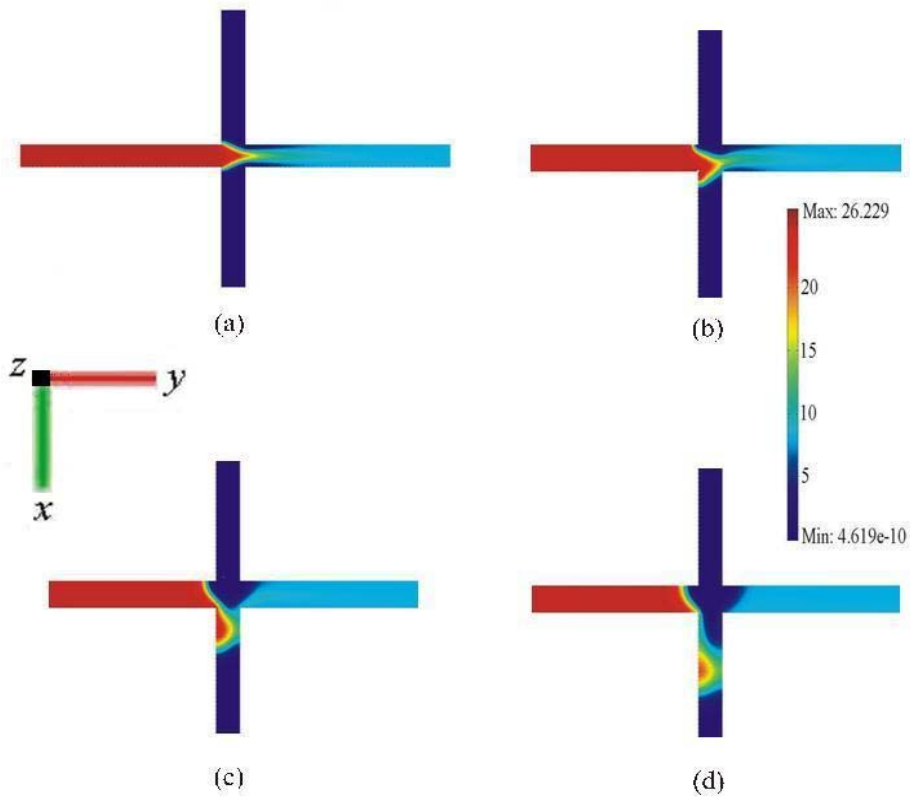

Figure 4: Sample concentration distribution (mol/m^3) at the plane $z = h/2$, for different times during injection process: (a) $t = 0$, (b) 0.2, (c) 0.4, and (d) 0.6 s. Numerical values for calculations are given in the text.

6 CONCLUSIONS

The formulation of a 3D finite element model of electro-osmotic flow is presented. The Navier-Stokes equation is coupled with the Poissson equation for electric potential via a slip velocity proportional to the electric field. This approximation is valid since the electric double layer thickness is very small compared with the width of the channel. Numerical values of fluid velocity were validated with exact calculations of electro-osmotic flow in channels of high aspect ratio l/w. Then, the transport of a sample composed of electrically neutral molecules is computed, emulating the operation modes known as focusing and injection. The concentration distribution maps obtained numerically show a remarkable qualitative agreement with the images obtained in experiments carried out under similar conditions (Li, 2004). Thus one may conclude that the 3D finite element model presented in this work is a valuable tool to control and optimize practical manipulations in microfluidic chips. Future directions in our work involve the transport of charges species, as well as the study of novel geometrical designs like double-cross microchannel systems (Yang, 2002).

ACKNOWLEDGEMENTS

The authors wish to thank the financial aid received from CONICET, Argentina. C.L.A.B. also acknowledges the financial support of SEPCYT-FONCyT, Argentina.

REFERENCES

F. Bianchi, R. Ferrigno, H. H. Girault. Finite element simulation of an electroosmotic-driven flow division at a T-junction of microscale dimensions. *Anal. Chem.*, 72:1987-1993, 2000.

D. Erickson and D. Li. Integrated microfluidic devices. *Anal. Chim. Acta*, 507:11-26, 2004.

D. Erickson. Towards numerical prototyping of labs-on-chip: modeling for integrated microfluidic devices. *Microfluid Nanofluid*, 1:301-318, 2005.

S. V. Ermakov, S. C. Jacobson, and J. M. Ramsey. Computer simulations of electrokinetic transport in microfabricated channel structures. *Anal. Chem.*, 70:4494-4504, 1998.

S. V. Ermakov, S. C. Jacobson, and J. M. Ramsey. Computer simulations of electrokinetic injection techniques in microfluidic devices. *Anal. Chem.*, 72**:**3512-3517, 2000.

M. Freemantle. Downsizing Chemistry *Chem. Eng. News*, 77**:**27-36, 1999.

L.-M. Fu, R.-J. Yang, G.-B. Lee. Electrokinetic focusing injection methods on microfluidic devices. *Anal. Chem.*, 75:1905-1910, 2003.

R. J. Hunter. *Foundations of Colloid Science*, volumes I and II. Clarendon Press, 1992.

D. Li. *Electrokinetics in Microfluidics.* Elsevier, 2004.

J.-Y. Lin, L.-M. Fu and R.-J. Yang. Numerical simulation of electrokinetic focusing in microfluidic chips. *J. Micromech. Microeng.*, 12**:**955-961, 2002.

J. M. MacInnes. Computation of reacting electrokinetic flow in microchannel geometries. *Chem. Eng. Sci.*, 57:4539-4558, 2002.

J. M. MacInnes, X. Du X and R. W. Allen. Prediction of electrokinetic and pressure flow in a microchannel T-junction. *Phys. Fluids*, 15:1992-2006, 2003.

M. Madou, *Fundamentals of Microfabrication, The Science of Miniaturization*, CRC Press, 2002.

N. A. Patankar and H. H. Hu. Numerical simulation of electroosmotic flow. *Anal. Chem.*, 70:1870-1881, 1998.

R. F. Probstein. *Physicochemical Hydrodynamics*. Butterworths, 1989.

D. R. Reyes, D. Iossifidis, P-A. Auroux and A. Manz, Micro Total Analysis Systems. 1. Introduction, Theory, and Technology, *Anal. Chem*., 74:2623 -2636, 2002.

H. A. Stone, A. D. Stroock and A. Adjari. Engineering flows in small devices: microfluidics toward lab-on-a-chip. *Annu. Rev. Fluid Mech*, 36:381-411, 2004.

N. Sundararajan, M.S. Pio, L.P. Lee, A. Berlin, Three-dimensional hydrodynamic focusing in polydimethylsiloxane (PDMS) microchannels, J MEMS 13:559–567, 2004.

R.-J. Yang , L.-M. Fu, G.-B. Lee, Variable-volume-injection methods using electrokinetic focusing on microfluidic chips, *J. Sep. Sci*, 25: 996–1010, 2002.